ELSEVIER

International Journal of Mass Spectrometry 214 (2002) 213–232

International Journal of Mass Spectrometry

www.elsevier.com/locate/ijms

Single and double cationization of organic molecules in SIMS

A. Delcorte[a,*], I. Wojciechowski[a], X. Gonze[a], B.J. Garrison[b], P. Bertrand[a]

[a] *PCPM, Université Catholique de Louvain, 1 Croix du Sud, Louvain-la-Neuve B1348, Belgium*
[b] *Department of Chemistry, The Pennsylvania State University, 152 Davey Lab, University Park, PA 16802, USA*

Received 4 September 2001; accepted 5 November 2001

Abstract

The cationization of sputtered organic species via metal particle adduction is investigated using a series of molecules and metallic substrates. Analyte molecules include styrene-based oligomers with various molecular weights, poly(methyl methacrylate) and a polymer additive. The chosen substrates are Al, Cr, Cu, Pd, Ag, In, Au and Pb. Metal-cationization occurs for all the substrates except Al. The cationized molecule yields vary strongly with the considered molecule and substrate and they are not correlated with the metal ion yields. In addition, double cationization with two metal particles is observed in specific cases (Cu, Pd, Ag, and Au supports, styrene-based polymers with ∼13 repeat units or more). The combination of electronic structure calculations, molecular dynamics and Monte-Carlo simulations supports an emission scheme in which excited molecules and metal atoms recombine above the surface and decay via electron emission, thereby locking the complex in the ionic state. (Int J Mass Spectrom 214 (2002) 213–232)

Keywords: Double cationization; SIMS; Monte-Carlo simulations; Polymers; Molecular dynamics; Electronic structure; Organometallic ions

1. Introduction

Static secondary ion mass spectrometry (SSIMS) is a powerful and versatile method for chemical surface analysis [1]. Still, as compared to other spectrometric techniques such as MALDI-MS and ESI-MS, the emission of large molecular ions remains an issue, for reasons that are inherent to the underlying physics of the method. Besides instrumental developments, several sample preparation strategies have been developed to favor the emission of high mass organic molecules. They involve the use of transition metal [2] or nitrocellulose substrates, the addition of 'ionizing' agents [3], the evaporation of an ultrathin metal layer on the sample [4] or the dissolution of the analyte in a low-molecular weight matrix [5], inspired by the MALDI procedure. The most widespread sample preparation procedure for large molecule analysis consists of depositing a sub-monolayer of analyte on a metal substrate [6–13]. In this context, *metal-cationization* denotes the complex process by which the molecule (M) and the metal (Me) combine and become ionized, leading to the formation of $(M + Me)^+$ species that can be detected by SIMS analyzers. The effect of the metal is actually two-fold. First, metallic substrates with a high atomic mass and a compact arrangement help to confine the projectile energy in the surface region and to reflect this energy towards the vacuum, which favors the desorption of analyte molecules [14,15]. Second, the metal substrate acts as an external source for analyte molecule ionization. Empirical studies have shown that the Ib group

* Corresponding author. E-mail: delcorte@pcpm.ucl.ac.be

1387-3806/02/$20.00
PII S1387-3806(01)00554-1

metal substrates (Cu, Ag, Au) provide the most efficient conjunction of characteristics for large molecule desorption and cationization [2].

The commonly accepted scenario for metal-cationization is that the ejected molecule *recombines* (i) *in the near surface region* (ii) with a metal *ion* (iii). This scenario has neither been demonstrated experimentally nor theoretically. Moreover, the existing body of experimental evidence does not seem entirely consistent [16]. Each one of the three points italicized in the above statement is still subject to discussion. First, the question arises whether the observed organometallic (M + Me) complexes are truly the result of a recombination or whether their constituents might be neighbors prior to emission and emitted 'as such', as is proposed for metal clusters [17–19]. To answer this question, molecular dynamic (MD) simulations providing a microscopic view of the emission process appear to be the method of choice [20]. The second point, related to the first one, questions *where* the association occurs: in the surface region (preformed complex), in the force field of the surface, where the sample can still act as an energy sink for the reaction, or out of influence of the surface, where the organometallic complex requires a specific route to evacuate the excess energy released by the exothermic association reaction. Recombination *far* from the surface, i.e., more than a few tens of nanometers, can be discarded a priori because the very low yield of emitted particles and the extreme localization of the emitting region for a kiloelectronvolt ion impact makes the probability of such an event close to zero.

Third, the rather intuitive view of the association involving a *neutral molecule* and a *metal cation* is also questionable. The absolute yields of metal cations are generally low, meaning that metal cation emission is a rare event as compared to neutral atom sputtering. The association of a metal cation with a sputtered molecule in the same bombardment event appears therefore problematic. In some cases, this hypothesis is totally inappropriate because the measured yield of cationized molecules is as high as 50 times that of metal ions, which suggests a recombination probability close to one [16]. Besides, the yields of metal-cationized molecules and metal cations are generally not correlated. The emission of cationized molecules has proven to be rather insensitive to the work function of the surface, in contrast with the metal ion yield, since silver cationized molecules can be sputtered with a similar intensity from metallic and oxidized silver surfaces [16]. The association of a metal ion with a neutral molecule also presents theoretical obstacles. If recombination occurs out of influence of the surface, the energy dissipated by the exothermic bond formation remains in the metal-molecule system, leading the molecule to a higher excitation state that will be prone to relax by fragmentation. If recombination occurs in the direct vicinity of the surface, where the substrate may act as an energy sink, the re-neutralization of the resulting ion is highly probable. Therefore, the depicted scenarios are not totally convincing.

In this paper, we tackle the issue of metal-cationization using results from experimental measurements, electronic structure calculations, classical molecular dynamics (MD) and Monte-Carlo (MC) simulations. Experimentally, most of the investigated molecules are based on the polystyrene (PS) structure, including regular PS oligomers with different mass distributions, polymethylstyrene and deuterated PS. For comparison, the cationization of a few other molecules with different chemical functionality is also explored. Eight metal substrates are compared. In the experimental results, it is shown that most of the studied metals induce cationization. Moreover, some of them induce a double cationization of the organic molecule by two metal ions. For comparison, the MD simulations involve short PS oligomers adsorbed on silver. They give us microscopic insights into the emission process as well as energy distributions for the desorbed molecules that compare to those obtained in the experiment. The MC simulations (TRIM) provide us with useful data concerning the sputtering yields of metal atoms for the chosen experimental conditions. Electronic structure calculations examine the interaction between the metal atom and the benzene ring, and its consequences for the ionization of PS molecules. The results obtained

from this combination of methods support a scenario of metal-cationization in which the excited molecule combines with a neutral metal atom and subsequently de-excites via electron emission.

2. Materials and methods

2.1. Samples

Samples of various organic molecules, including several low molecular weight polymers, are dissolved with a concentration of 1 mg/mL. The nature and origin of the chosen molecules, as well as the solvents used for their dissolution, are listed in Table 1. The samples are prepared as thin films cast on 0.25 cm^2 substrates by depositing a droplet of the solution on the supports. As indicated in Table 2, the substrates are either thin metal foils or metallized supports. The metallized substrates are prepared by evaporating a 100 nm layer of the chosen metal (Al, Cr, Ag, Au) on clean silicon wafers. The evaporation is carried out in an Edwards evaporator at an operating pressure of $\sim 5 \times 10^{-6}$ mbar and a deposition rate of 0.1 nm/s. Prior to organic sample deposition, all the substrates are etched in 30% highest purity grade sulfuric acid (Vel) for 3 min, then rinsed in high-performance liquid chromatography (HPLC) grade water from a milli-Q system (Millipore) and p.a. grade isopropanol (Vel).

Table 2
Characteristics of the sample substrates

Substrate	Nature
Aluminum, Al	Evaporated on Si (100 nm)
Chromium, Cr	Evaporated on Si (100 nm)
Copper, Cu (99.9% pure)	Foil (500 μm)
Palladium, Pd	Foil (1 mm)
Silver, Ag (99.95+ % pure)	Foil (100 μm)
	Evaporated on Si (100 nm)
Indium, In (99.999% pure)	Foil (500 μm)
Gold, Au	Evaporated on Si (100 nm)
Lead, Pb (99.95% pure)	Foil (500 μm)

2.2. Secondary ion mass spectrometry (SIMS)

The secondary ion mass analyses and the KED measurements are performed in a PHI-EVANS time-of-flight (ToF)-SIMS (TRIFT 1) using a 15 keV Ga^+ beam (FEI 83-2 liquid metal ion source; ~600 pA DC current; 22 ns pulse width bunched down to ~1 ns; 4 kHz repetition rate) [21]. The experimental setup has been described in detail elsewhere [22]. To improve the measured intensities, the secondary ions are post-accelerated by a high voltage (7.5 kV) in front of the detector. ToF-SIMS spectra in the mass range

Table 1
Characteristics of the analyzed molecules

Molecule	Abbreviation	Molecular weight (M_n)	Origin	Solvent
Small hydrocarbons				
Triacontane	TC	423	Sigma-Aldrich NV/SA, Bornem	Benzene
Tetraphenylnaphtalene	TPN	433	Sigma-Aldrich NV/SA, Bornem	Benzene
Polymers				
Polystyrene	PS700	700	Scientific Polymer Products Inc., Ontario	Toluene
Polystyrene	PS1100	1100	CERM, University of Liège	Toluene
Polystyrene	PS2180	2180	Scientific Polymer Products Inc., Ontario	Toluene
Polystyrene	PS5120	5120	Scientific Polymer Products Inc., Ontario	Toluene
Poly-4-methyl styrene	P4MS	3930	University of Louvain	Toluene
Deuterated polystyrene	PSD	5300	Polymer Standard Services, Mainz	Toluene
Polymethyl methacrylate	PMMA	3800	University of Louvain	Dichloromethane
Additives				
Irganox 1010	Irganox	1176	Ciba Specialty Chemicals Inc., Basel	Toluene

$0 < m/z < 10{,}000$ are obtained from 1200 s acquisitions on a 130 μm × 130 μm sample area, which corresponds to a fluence of 1.1×10^{12} ions/cm^2, ensuring static bombardment conditions. It is important to note that, with the current detector mounted on the ToF-SIMS instrument and the chosen post-acceleration voltage, the detection of dications is favored over that of monocations. The reason is two-fold: first, for monocations, the efficiency of this detector decreases dramatically beyond 2 kDa, and second, dications receive two times more energy than monocations in the post-acceleration section, which specifically increases their detection probability.

2.3. Monte-Carlo simulation (TRIM code)

A Monte-Carlo code based on the binary collision approximation (TRIM [23]) is used to calculate the sputtering yield of atoms from various metals and oxides bombarded by 12 keV Ga ions. The results have been obtained with the SRIM version of the code (information concerning this program can be found at the following internet address [24]). A thousand trajectories were fully calculated for each substrate used in the experiment (Table 2). Calculations have also been performed with the native oxide form of the metal substrates. The parameters related to the substrates (density, surface barrier energy) were found in the compound library of the software and the literature [25]. For noble metals, the metal/oxygen ratio used for the oxidized surface in the model derives from X-ray photoelectron spectroscopy measurements. The size of the cell has been chosen in order to include the whole ion and cascade atom trajectories for each set of bombardment conditions (500 Å).

2.4. Classical molecular dynamics (MD)

The Ar bombardment of *sec*-butyl terminated PS oligomers adsorbed on a Ag(1 1 1) surface is modeled using MD computer simulation. The details of the simulation have been described elsewhere [14,15]. Briefly, the first sample consists of 13 PS *tetramers* (four styrene repeat units) placed on the Ag(1 1 1) surface (12 layers of 528 atoms each). The second sample consists of one central PS tetramer surrounded by two PS *hexadecamers* or 16-mers (16 styrene repeat units), placed on the same Ag crystal. The systems are quenched to a minimum energy configuration prior to Ar atom impact. A total of 500 trajectories directed along the surface normal were calculated with the first sample. Trajectories of interest characterized by high action and high yield were recalculated with the second sample. The simulation consists of integrating Hamilton's equations of motion over some time interval to determine the position and velocity of each particle as a function of time. The energy and forces in the system are described by many-body interaction potentials, in particular, the C–C, C–H and H–H interactions are described by the Brenner potential function [26,27]. The criterion for terminating the trajectory is that the total energy of any atom is too low to induce ejection. The termination times range from 0.5 to 6 ps, depending on the manner in which the energy distributes in the solid. Experimentally observable properties, such as total yield, mass spectrum, kinetic energy, and angular distributions are calculated from the final positions, velocities, and masses of all the ejected species. Mechanistic information is obtained by monitoring the time evolution of relevant collisional events.

2.5. Electronic structure calculations

Electronic structure calculations are performed in order to establish the potential energy vs. distance curves for the C_6H_6 + Ag system [28]. For this purpose, we use the generalized gradient approximation (GGA) implemented in the ABINIT code.[1] Real ion–electron interaction potentials are replaced by the GGA-based pseudopotentials generated with the Fritz Haber Institute code [32]. In these calculations, the

[1] ABINIT is a common project of the Université Catholique de Louvain, Corning Incorporated and other contributors (http://www.pcpm.ucl.ac.be/abinit). It relies on an efficient fast Fourier transform algorithm [29] for the conversion of wave functions between real and reciprocal space, on the adaptation to a fixed potential of the band-by-band conjugate gradient method [30], and on a potential-based conjugate-gradient algorithm for the determination of the self-consistent potential [31].

neutral and ionic states of the silver atom are considered within a standard ground-state total energy framework while the excited state ($4d^9 5s^2$) is obtained within the ΔSFC (self-consistent field) framework [33]. As a preliminary check, we calculated the ionization potential of Ag and the excitation potential for the Ag($4d^9 5s^2$) state, which are respectively 6.98 and 3.96 eV, in reasonable agreement with experimental values (7.59 [34] and 3.75 eV [35,36], respectively). The geometry optimization for benzene, conducted using the Broyden–Fletcher–Goldfarb–Shanno algorithm [37], gives C–C and C–H bond lengths that differ from the experimental values by less than 1%. The calculation of the equilibrium distance and potential well depth between the benzene ring plane and the Ag^+ ion approaching along the C_6 axis provide us with an optimum distance of 2.272 Å and a binding energy of 1.74 eV, in agreement with the experiment [38].

3. Results and discussion

In Section 3.1, we introduce a study of metal-cationized molecules via the ToF-SIMS technique. The measured mass distributions and ion yields are commented. Throughout the section, we emphasize the new observations related to doubly cationized molecules. In Section 3.2, the formation mechanism of singly and doubly cationized molecules is explored using Monte-Carlo, classical molecular dynamics and electronic structure calculations.

3.1. Experimental observations

3.1.1. The molecule-metal cluster spectra

The major experimental results of this study will be highlighted via the case of PS2180, a *sec*-butyl terminated PS sample with a number average molecular weight $M_n = 2180$ Da. The mass spectra corresponding to the adsorption of PS2180 on several metal substrates are shown in Fig. 1a and b.

3.1.1.1. General description. Fig. 1 focuses on the high mass range of the mass spectrum, where entire cationized molecules can be found. First, the familiar distribution of peaks induced by the metal-cationization of entire styrene oligomers with different repeat unit numbers is observed for all the metal substrates, except aluminum. In that sense, copper, silver and gold are not an exception among the large family of metals. Metallic substrates as different as chromium(VIa), palladium(VIII), indium(IIIb) and lead(IVb) also induce molecule cationization. Nevertheless, different substrates are characterized by different cationized parent ion yields, as is shown in the next section. Besides the main peak distribution, other peaks appear with more or less intensity according to the nature of the substrates. Some of them correspond to cationized fragments, which have been studied in a previous article [39].

In addition to the distributions of cationized molecules and fragments, one clearly notices a third series of peaks in the cases of the copper, silver and gold substrates. This series is labeled by stars in Fig. 1. It peaks around 1100 Da and the mass difference (Δm) between two consecutive peaks in the series is 52 Da. The mass assessment procedure shows that the peaks of this distribution correspond to the formula $(M + 2Me)^{2+}$. This identification is confirmed by the position of the distribution maximum, that is about half the mass of the cationized parent distribution, and by Δm, that is half the mass of the styrene repeat unit, because of the double positive charge of these ions. For the sake of simplicity, this series of peaks is called the *dication distribution* in the rest of this paper. A more detailed analysis shows that metal-molecule dications are also sputtered from palladium substrates but with a much lower efficiency (Fig. 1a). There is no detectable contribution of $(M + 2Me)^+$ monocations in any of the spectra.

3.1.1.2. Structure of the distributions. In Fig. 2, we compare the yields of metal-molecule monocations, dications and cationized fragments as a function of the styrene repeat unit number for silver substrates. The cationized oligomer distribution peaks at 17 repeat units and vanishes beyond 30 repeat units. Remarkably, there is also an intensity increase towards smaller

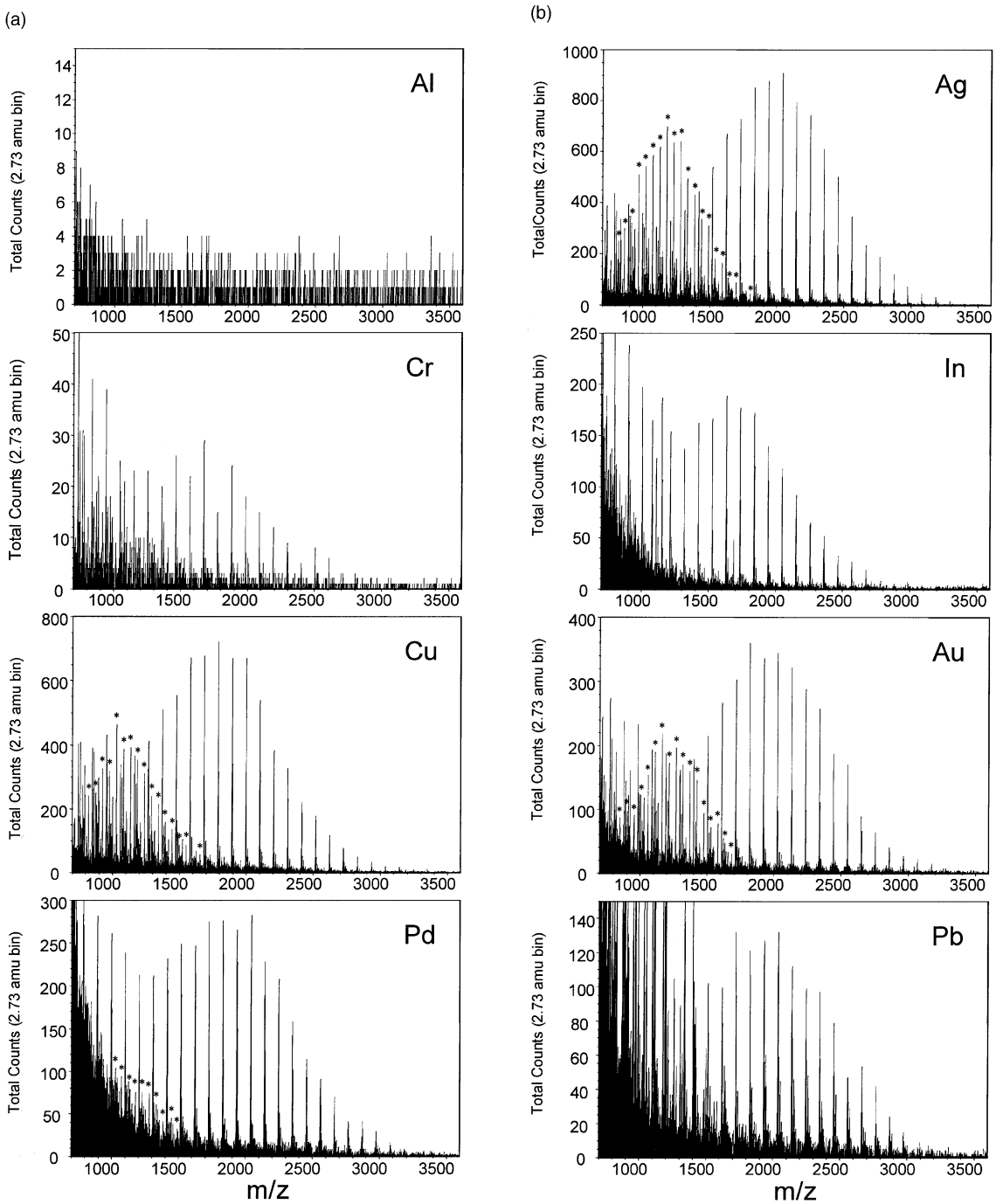

Fig. 1. High mass range of the ToF-SIMS spectra for PS2180 adsorbed on different substrates: (a) Al, Cr, Cu, Pd; (b) Ag, In, Au, Pb. The stars indicate $(M + 2Me)^{2+}$ complexes.

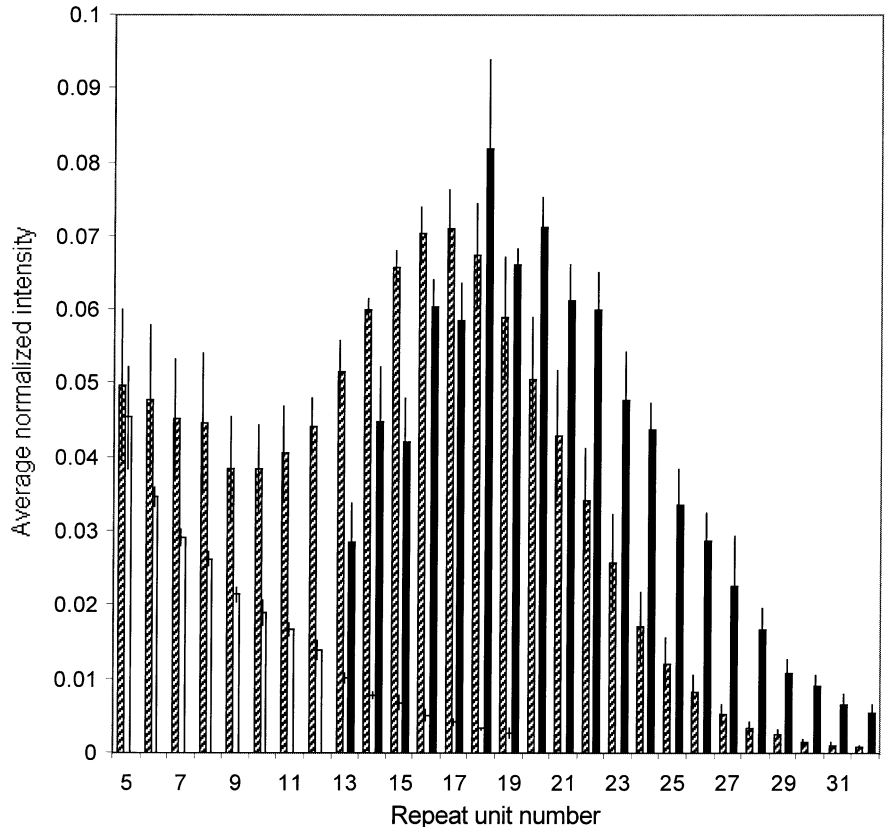

Fig. 2. Molecule-metal cluster distributions for PS2180 adsorbed on Ag. Dashed bars: singly cationized molecules, including cationized *sec*-butyl-terminated fragments (see text for details); full black bars: doubly cationized molecules; empty bars: cationized H-terminated fragments.

molecular weights, so that a minimum is observed for 9–10 styrene repeat units. In contrast with the monocation distribution, the dication distribution starts rather abruptly at 13 repeat units, peaks around 20 repeat units and extends beyond 32 repeat units. The calculated M_n is 2155 Da for the dication distribution and 1585 Da for the cationized parent distribution. For comparison, the M_n provided by chromatography is 2180 Da. Therefore, the average molecular weight deduced from the dication distribution most closely matches the chromatographic value.

3.1.1.3. Fragmentation. Fig. 2 also shows the distribution of cationized fragments formed by the loss of the *sec*-butyl endgroup plus a number of repeat units. Each of these fragment peaks probably originates from several precursors with different sizes. The cationized fragment intensities increase monotonically with decreasing repeat unit number. For five repeat units, it is similar to the intensity of the corresponding peak of the parent distribution.

Fragmentation helps us to interpret the intensity decrease observed in the parent distribution below nine styrene repeat units. For PS oligomers terminated by hydrogen at one end, it is impossible to separate the cationized parent distribution from the distribution of cationized fragments formed via the loss of the H endgroup plus *k* repeat units. Indeed, a backbone cleavage of molecule M1 with retention of the charge and silver atom on the *sec*-butyl side of

the molecule will generate a distribution of fragments with the mass $m_{M1} + m_{Ag} - k \times 104$ Da, which is also equal to $m_{M2} + m_{Ag}$, M2 being an intact oligomer shorter than M1 by k repeat units. In contrast, fragments resulting from the loss of the *sec*-butyl endgroup plus a number of repeat units constitute a distinct distribution, shown in Fig. 2. Assuming that fragments with the H endgroup and fragments with the butyl endgroup are generated with equivalent probabilities in the different dissociation scenarios, they should have similar intensities in the mass spectrum. That is exactly what is observed for fragments with five repeat units, where the influence of the parent molecule intensity is negligible. Therefore, we believe that the low mass part in the cationized parent distribution, below nine repeat units, is an artefact induced by the fragmentation of metal-molecule cations and/or dications. Subtracting the fragment distribution from the apparent parent distribution should yield the true distribution of intact molecules. Using this procedure, the calculated M_n becomes 1769 Da for the cationized parent distribution. It should be noticed that this estimate is still lower than the chromatographic value.

3.1.1.4. Molecule-metal dications. One intriguing feature of the dication distribution consists in its lack of low mass oligomers. The absence of short oligomer dications is confirmed by Fig. 3, which shows the mass spectra of a PS oligomer sample with $M_n = 700$ Da. The same observation applies to a PS oligomer sample with $M_n = 1100$ Da. This effect is probably a consequence of the electrostatic repulsion between same sign charges. Indeed, for molecular dications, the shorter the molecule, the stronger the repulsive force between the metal cations. It is reasonable to think that, below a threshold molecular size, the repulsive potential is large enough to prevent the formation or to affect the stability of dications.

In a similar manner, the fragments identified in the mass spectra could also be induced by the decomposition of metal-molecule dications, with retention of one positive charge by each fragment. In fact, there is some indirect indication that dications are a significant

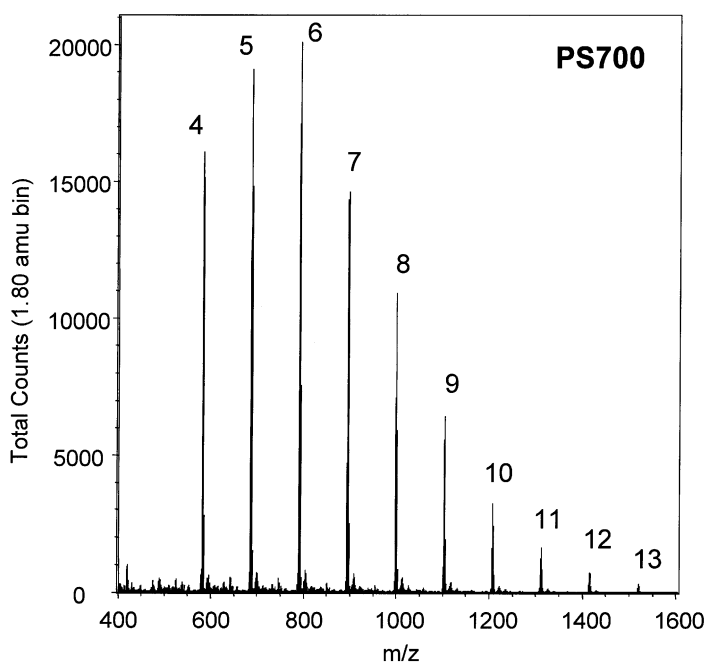

Fig. 3. High mass range of the ToF-SIMS spectrum for PS700 adsorbed on Ag.

source of singly charged fragments. First, Fig. 1 qualitatively shows that the amount of fragments detected in the singly cationized oligomer distribution is low when the intensity of dications is high, and vice-versa. Second, the mass distribution of PS700 (Fig. 3) and PS1100, where dications are not observed at all, exhibit very weak fragment intensities. These two observations are consistent with the hypothesis that dications decompose and give rise to singly charged fragments.

On the other hand, dications are observed for higher mass oligomers and for other molecules than regular PS. In particular, we measured their distribution for PS5120, PSD and P4MS. The corresponding regions of the mass spectra are shown in Fig. 4 for these three samples. Neither the replacement of hydrogen by deuterium atoms in the PS molecule nor the addition of a methyl functionality to the phenyl pendant group of PS prevent the formation of dications. The number average molecular weights calculated from the dication distributions are 4832 Da for PS5120, 4700 Da for PSD and 3814 Da for P4MS. These values are respectively 6, 11 and 3% lower than the reported chromatographic values.

3.1.2. Useful yields of cationized molecules

The useful yields of sputtered ions have been calculated using the primary and secondary ion currents measured in the experiments. The yields of metal-molecule cations and dications are summarized in Table 3 for the entire set of investigated substrate-molecule pairs. In Table 3, the yields are symbolized by capital letters (see Table 3 legend). The choice to report ranges of yields instead of exact numeric values is motivated by the significant yield variation observed for different samples cast from the same solution.

3.1.2.1. Effect of the molecular weight. Comparing values in individual columns of data in Table 3, it is apparent that the measured yields are larger for short molecules than for long molecules, irrespective of the substrate. However, it is imprudent to draw any definitive conclusion from that observation because the

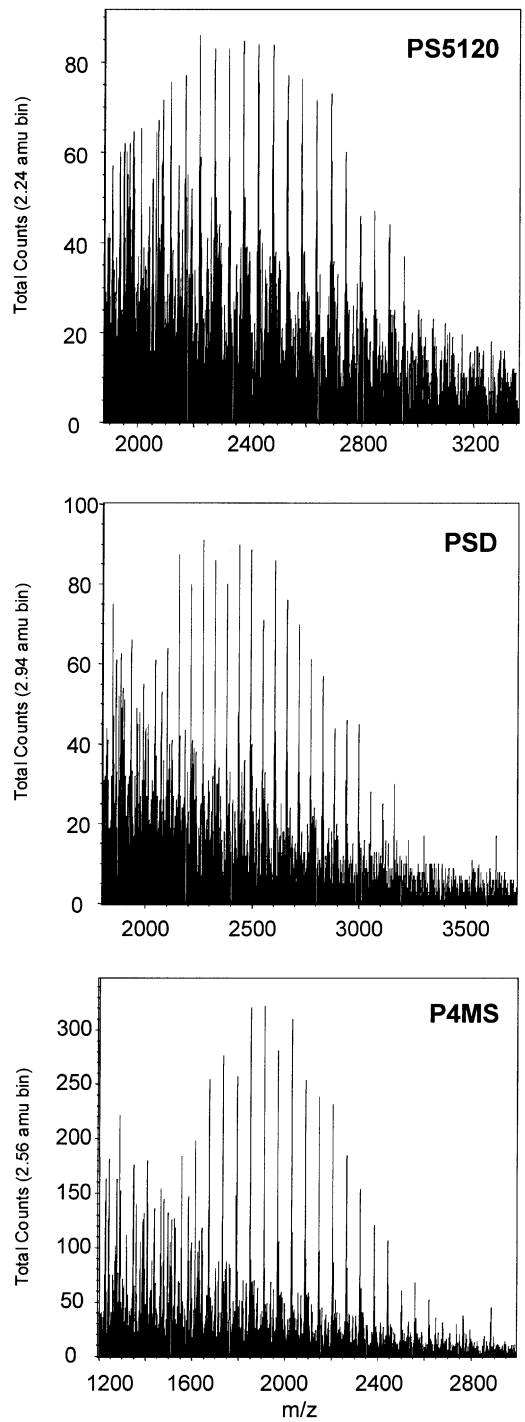

Fig. 4. High mass range of the ToF-SIMS spectra for PS5120, PSD and P4MS adsorbed on Ag.

Table 3
Useful ion yields (Y) of metal-molecule monocations and dications for different analytes and substrates

	Al (27)	Cr (52)	Cu (64)	Pd (106)	Ag (108)	In (115)	Au (197)	Pb (207)
Monocations								
TC(423)			A		A		A	
TPN(433)			A+		A+		A+	
PS700					A/A+			
PS1100					A			
PS2180	None	D	B	C	A/B	C	B	C
PS5120					D		D	None
P4MS(3933)		None	C/D	D	C/D		C/D	
PSD(5300)					D			
Irganox(1176)			A	A	A+		A	
PMMA(3800)					D			
Dications								
PS2180	None	None	B	D	B	None	B	None
PS5120					C/D		C	None
P4MS(3933)		None	C	None	C		C	
PSD(5300)					C/D			

A+: $Y \geq 10^{-4}$; A: $10^{-5} \leq Y \leq 10^{-4}$; B: $10^{-6} \leq Y < 10^{-5}$; C: $10^{-7} \leq Y < 10^{-6}$; D: $10^{-8} \leq Y < 10^{-7}$. The numbers in parenthesis are the metal and molecule atomic weights.

detection efficiency of the analyzer decreases with secondary ion mass in a manner that is not well known. Nevertheless, it is of practical interest to remark that for molecules with the same chemical structure, e.g., polystyrene oligomers, about one order of magnitude in yield is lost when the mass increases from ∼700 to 2200 Da. More than one order of magnitude is lost again between molecules of ∼2200 and 5100 Da. As a consequence, it is hazardous to derive molecular weight numbers from broad cationized oligomer distributions. In addition, with the detector used in our experiments, it is almost impossible to analyze species with a molecular weight larger than 3–5 kDa, depending on the chemistry of the compound. The intensity decay of dications as a function of molecular weight is lesser than that of monocations. One reason of this behavior is that their kinetic energy is twice that of monocations, which contributes to enhance the detection efficiency for a given mass. Therefore, the analysis of dications constitutes a means to expand the accessible mass range in SIMS for the considered class of materials.

3.1.2.2. Effect of the analyte nature. Other observations provide less ambiguous information about the cationization efficiency. First, for the set of samples tested in this study, cationization occurs whatever the chemical functionalities present in the molecule. Second, for similar masses, molecules with phenyl pendant groups are cationized 3–10 times more efficiently than molecules without a phenyl ring (TPN vs. TC; P4MS vs. PMMA). An almost complete deuteration of the molecule or the addition of a methyl residue to the phenyl pendant group have no effect on the cationization and dicationization efficiencies (PSD and P4MS vs. PS5120). Although their chemical formulae differ significantly, PS1100 (∼10 phenyl rings) and irganox (four phenyl and four carboxyl groups) have comparable yields for single cationization, considering that the entire distribution is taken into account instead of the yield of the most abundant oligomer for PS1100. Third, dications are observed with significant yields (B–D) only for molecules including phenyl rings (PS, PSD, P4MS), and for molecular weights above 1.2 kDa.

3.1.2.3. Effect of the substrate nature. The analysis of Table 3 also allows us to classify the substrates with respect to their efficiency towards cationization. Silver and gold are very efficient, followed by copper,

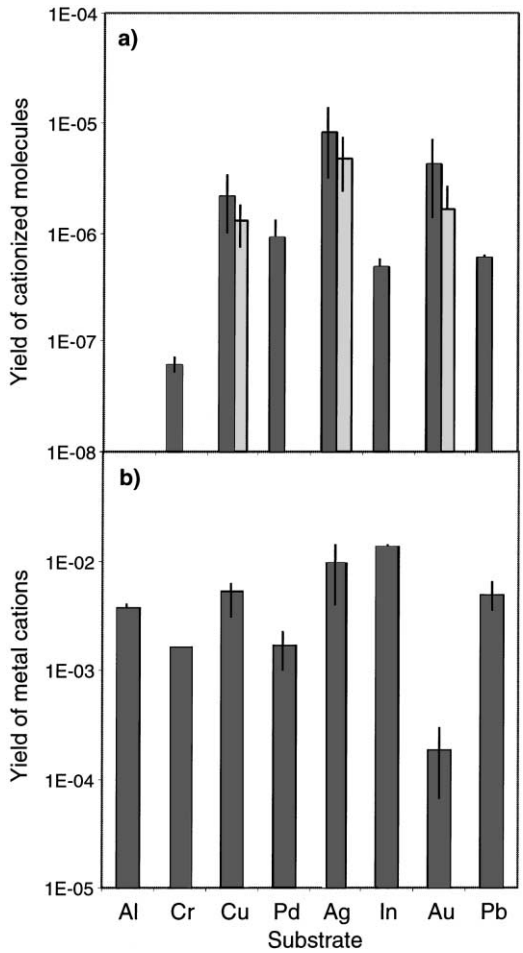

Fig. 5. Useful ion yield of (a) molecule-metal monocations (black bars) and dications (gray bars); (b) atomic silver ions sputtered from PS2180 adsorbed on Ag.

palladium, indium and lead. Chromium has a significantly lower efficiency and aluminum does not cationize at all. This effect is reflected by the bargraph of Fig. 5a, where the absolute values of the yields of metal-molecule cations and dications are shown for the eight considered substrates. These yields refer to the 18-mer in the distribution of PS2180, i.e., the most abundant oligomer for most of the chosen substrates (see Figs. 1 and 2). The error bar corresponds to the standard deviation calculated for at least three to five measurements. The trend is similar for dications, observed for group Ib substrates (Cu, Ag, Au) and to a lesser extent, for palladium substrates. The yield of dications is not reported for palladium substrates because the corresponding signal to noise ratio is very small.

For comparison, the measured yield of atomic metal cations is plotted in Fig. 5b. It is lower than 10^{-2} and does not correlate at all with the yield of metal-cationized molecules or dications. It is particularly obvious when comparing substrate pairs such as copper and gold or palladium and indium. As discussed in Section 3.2, it is an important point regarding the physical explanation of the cationization process, because it constitutes an obstacle to the concept of recombination between a neutral molecule and a metal cation. According to this concept, the evolution of $(M + Me)^+$ species and Me^+ cations should be somehow correlated.

3.2. Mechanisms

In this section, the experimental results involving cationization are interpreted on the grounds of Monte-Carlo, molecular dynamics and electronic structure models. The desorption–recombination phase of the process is addressed in the first subsection and an associative ionization mechanism is proposed in the second subsection to account for the observation of singly and doubly cationized molecules.

3.2.1. Desorption and recombination

The formation of organometallic ions requires the concerted transfer of organic molecules and metal atoms from the solid phase to the vacuum in a single bombardment event. Molecular dynamics simulations help us identify the most probable scenario for the creation of metal-molecule complexes.

First, let us examine the condition and characteristics of large organic molecule and cluster emission under kiloelectronvolt ion bombardment. The important features of the emission mechanism are exemplified in Fig. 6 for different bombardment events (5 keV Ar projectiles). Fig. 6a shows that the concerted emission of several PS tetramers (∼500 Da) and numerous silver atoms occurs in the simulation. Such a scenario is

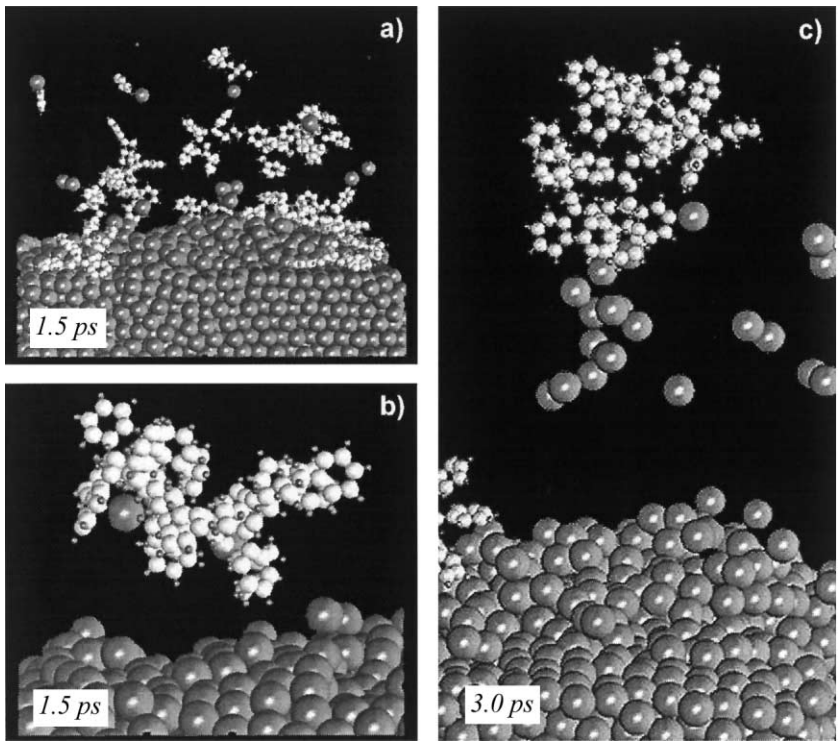

Fig. 6. Snapshots of MD simulation movies. (a) High action event ejecting styrene tetramers and silver atoms and clusters; (b) Close-up view of a styrene 16-mer recombining with a silver atom close to the sample surface; (c) Concerted emission of a styrene 16-mer with metal atoms and clusters.

not rare. As shown in a recent study based on a representative sample of 500 trajectories [15], ∼35% of the trajectories eject as much as three PS tetramers and seven Ag atoms in a single event. Even though ions are not described by the model, the molecular dynamics indicates a probable scenario for metal-molecule complex formation. In the simulation, the departing molecules are sometimes followed by a silver atom initially located in the direct vicinity of the molecule. A few angstroms above the surface, the metal atom and the molecule gather, forming the complex. Such a mechanism is less *frequent* for larger PS oligomers (∼2 kDa), as explained hereafter, but the calculated trajectories also show that it constitutes the main route to form organometallic complexes. The process is illustrated in Fig. 6b for a 16 repeat unit PS oligomer. After 1.5 ps, the PS molecule is accompanied by a silver atom trapped by its chain segments. The last vignette of Fig. 6 shows that high action events in the surface can also lead to the concerted emission of a PS molecule together with several substrate atoms or clusters.

Molecular dynamics simulations conducted for different systems, using statistically representative sets of trajectories [14,40–42], show that the desorption efficiency and, to some extent, the desorption mechanisms depend on the molecular size. For relatively small molecules up to 500 Da at least, desorption can be easily caused either by quasi-one atom collisions or by a co-operative uplifting mechanism involving several substrate atoms [14]. However, the simulation results clearly show that the higher the mass of the molecule, the more difficult it is to desorb it from the surface. For example, the yield of benzene molecules (78 Da) sputtered under 500 eV Ar bombardment is more than two times larger than that observed for dibenzanthracene

molecules (278 Da) and about ten times greater than that of PS tetramers (474 Da) ejected in the same conditions. The desorption of a 2 kDa oligomer occurs even less frequently and it needs the collective upward motion of several metal atoms underneath the molecule [15]. Moreover, sputtering calculations using 5 keV Ar atoms as projectiles show that the large-scale collective motions which are capable of desorbing 2 kDa oligomers are not sufficient to transfer a 7 kDa PS oligomer in the vacuum.

In practice, the above-mentioned mass dependence of the desorption efficiency should lead to sputtered molecule distributions that do not mirror the real molecular weight distribution of the polymer. In contrast, it has been reported in the literature that the experimental results concerning Ag-cationized oligomer distributions usually correlate with chromatographic determinations of the average molecular weight (within a 10% error range [43]). This apparent contradiction between calculated and experimental results can be alleviated if the metal-molecule association efficiency increases with the molecular weight, in order to (partly or totally) compensate for the desorption efficiency decrease. It is a reasonable hypothesis, because heavier molecules, covering larger areas on the sample surface, should naturally exhibit larger association cross-sections. In this interpretation, the different shapes of the distributions shown in Fig. 1 could suggest that the mass-dependent variations of the desorption and cationization efficiencies do not always compensate exactly and that they are a function of the substrate nature. Silver could then be a substrate for which the two inverse trends almost cancel one another.

3.2.2. Ionization

MD simulations show that organic molecules and metal particles primarily associate above the sample surface [14,15,44], as part of a collective emission process. As explained in the introduction, a cationization process based on the recombination of a neutral molecule with a metal ion is probably insufficient in terms of yields. Our results bring additional arguments against this hypothesis.

First, the yields of metal ions are low in the experiments considered in Section 3.1. As shown in Fig. 5b, they vary between 10^{-4} (Au) and 10^{-2} (In). Considering additional constraints in time, space and velocity vectors, the association of metal ions and neutral molecules should be a very low probability event. Second, the yields of cationized molecules and metal ions are not correlated for the considered set of substrates. Finally, if single cationization by a metal ion is a very low probability event, double cationization of a given organic molecule by two independent metal cations, as observed for several metals with a very significant yield, is obviously not realistic.

Therefore, we propose that neutral molecules recombine with metal atoms rather than ions [28]. In this context, ionization of the nascent complex can occur via ejection of an electron during the association process (Hornbeck–Molnar process [45]). The process of associative ionization is described by Eq. (1)

$$A^{(*)} + B \rightarrow AB^{+} + e^{-}. \quad (1)$$

In the course of the recombination reaction, the two constituents may approach closely enough to pass a crossing between the neutral and ion potential energy curves. At this point, the complex becomes auto-ionizing and the ejection of an electron is favored. Considering the cationization of an organic species, the functional groups (e.g., phenyl) of the molecule and the metal atom will be the reactants. The emission of an electron according to Eq. (1) constitutes a way to dissipate the energy released by the reaction. Once the electron is ejected, the isolated complex is locked in the ionic state.

Qualitatively, two slightly different scenarios can be considered, depending on the state of the silver atom. In the first scenario, a part of the energy needed to overcome the reaction barrier is provided by the metal atom, which is in an excited state. Detailed electronic structure calculations are presented for this case in the discussion. In the second scenario, the required energy is brought by the vibrationally excited organic molecule and the metal atom lies in the ground state. If it is energetically equivalent, the second scenario should be favored because the number of ground state

atoms is at least one order of magnitude larger than that of excited atoms. In the following paragraphs, we develop several arguments in favor of the associative ionization process, and we comment on the validity of the different scenarios.

3.2.2.1. Yields of metal atoms. According to our hypothesis of cationization, sputtered neutral molecules recombine with metal atoms instead of ions. First, this hypothesis has the merit that the metal atom yields are often greater than those of ions by several orders of magnitude. Therefore, it is easily conceivable that metal atoms and organic molecules sputtered in a single event recombine above the surface, as shown in Fig. 6.

A Monte-Carlo sputtering code using the binary collision approximation (TRIM) has been used to calculate the sputtering yields of the considered metals under 12 keV Ga ions at oblique incidence, i.e., the exact bombardment conditions of our experiments. Indeed, in our ToF-SIMS, the 15 keV Ga ions approaching the surface are decelerated and deflected by the 3 kV potential of the sample holder, so that their final impact energy and angle of incidence are 12 keV and 40°. Fig. 7 shows the sputtering yields of metal atoms calculated by TRIM for the considered samples. Because of the sample preparation method, the surface of the real samples is partially oxidized. Therefore, we report the metal atom yields for the different metals and for their oxides. The yields vary between 10 and 18 for the pure metals, and between 4 and 13 for their native oxides. Although data have not been reported for these particular bombardment conditions, our values agree qualitatively with published experimental results [46]. Remarkably, the calculated neutral yields are 10^2 (Ag, In) to 10^5 (Au) times larger than those *measured* for metal ions (Fig. 5b). Even though the transmission of our instrument is not 100%, the calculated neutral yields certainly remain on average several orders of magnitude larger than the *real* ion yields. In contrast with cations, metal atoms constitute an important reservoir of particles that can participate to the cationization process. The calculated yields of Fig. 7 can be compared to the measured yields of

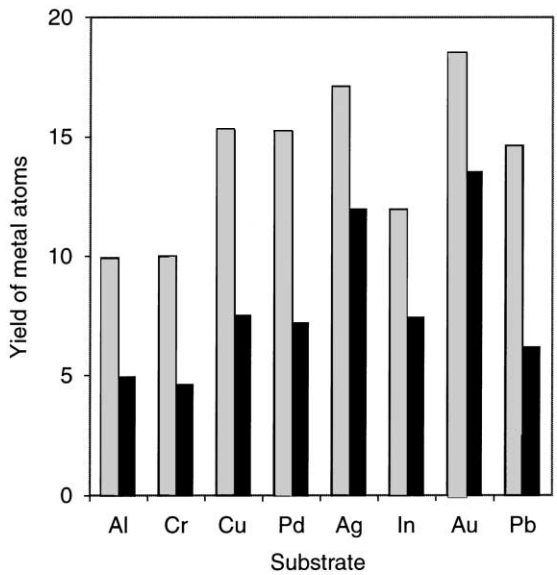

Fig. 7. Sputtering yield of metal atoms calculated by TRIM for pure metal (gray bars) and metal oxide (black bars) surfaces.

metal cationized molecules presented in Fig. 5a. Even though the yield variation is larger for the metal cationized molecules, the two patterns bear a resemblance that is not observed with metal ions (see for instance the series Pd–Ag–In–Au–Pb).

It may appear questionable to compare metal yields obtained in the BCA scheme with cationized molecule yields, since we know that kDa molecules require co-operative many-body interactions in the metal surface to be desorbed. A double argument can be invoked to answer this objection. First, the average yield values provided in the BCA approximation for sputtered atoms compare well with experimental values reported in the literature. More importantly, the number of subcascades, of atomic displacements and the energy dissipated by the projectile in the surface region, identified as the cause of large sputtering events, vary as a function of the sample nature and bombardment conditions in a manner that is qualitatively similar to more refined models such as the MD simulations. Therefore, even though collective events do not exist in the BCA scheme, dense cascades may occur in the surface region, and they induce sputtering yields

that are higher than the average, as is the case in the MD simulations.

In the introduction of this section, we propose two associative ionization scenarios, depending on whether the metal atom is in a ground or an excited state. The TRIM code does not provide us with excited state atom fractions and an exhaustive experimental study involving all the substrates used in this article does not exist yet. Nonetheless, some hints concerning the metastable atom fractions can be found in the recent literature. Berthold and Wucher showed that Ag* ($4d^9 5s^2$, $D_{5/2}$) atoms, the most abundant among the excited atoms sputtered from clean Ag surfaces, represent up to 6% of the neutral flux [47]. Similar populations have been found for metastable Cu atoms [48]. These values are still much larger than the ion fractions sputtered from the same surfaces. Therefore, this scenario appears as relevant and will be considered in detail hereafter.

3.2.2.2. Associative ionization in the vacuum. To check the feasibility of the associative emission process, we performed first principle calculations in GGA, using the C_6H_6–Ag system as a model for the interaction between PS oligomers and silver atoms [28]. The potential energy curves have been calculated for the neutral, charged and excited system $C_6H_6 + Ag^{0/+/*}$. The considered excited state of the silver atom is [$4d^9 5s^2$], because it corresponds to the predominant fraction of excited atoms sputtered from Ag surfaces [47]. Geometrically, the silver atom approaches the benzene ring along the C_6 symmetry axis.

The calculated potential energy curves are plotted in Fig. 8 as a function of the distance between the Ag atom and the benzene ring along the C_6 axis. The excited states of the silver atom, corresponding to the promotion of a d-electron, are split in the benzene field into three distinct potential energy curves. Two of them, corresponding to the transitions from the lowest energy still degenerate $d_{x^2-y^2}$ and d_{xy} orbitals (upper curve), and from the highest energy degenerate d_{xz} and d_{yz} orbitals (lower curve), to the 5s orbital, are shown. The potential curve for the transition from

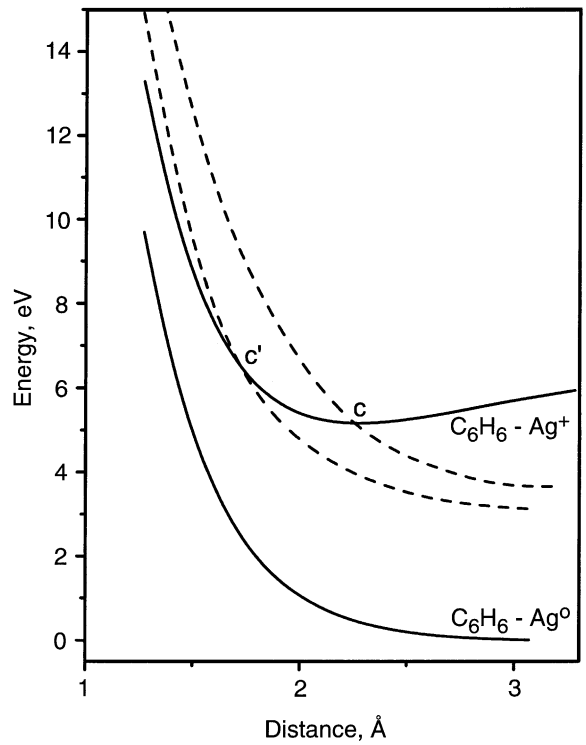

Fig. 8. Potential energy curves for the model system $C_6H_6 + Ag$. Solid curves correspond to the ground state (lower) and the ionic state (upper). Excited states are indicated by dashed curves. The curve crossings between the excited and ionic states of the complex are indicated by letters *c* and *c′*. Electronic transitions are labeled with letters *a*, *b* (see text for details).

the d_{z^2} orbital (not shown) should be between the two other curves. It has not been calculated because the ΔSCF procedure is extremely time consuming.

The fact that no crossing exists between the neutral *ground* state and the ionic state of the system indicates that associative ionization cannot occur in the vacuum for ground state Ag atoms. Nevertheless, Fig. 8 also shows that crossings (*c*, *c′*) occur between the *excited* states and ionic state of the system. At this point, the association of the constituents, accompanied by the ejection of an electron, becomes thermodynamically favorable. From the potential energy diagrams, we can deduce that the potential barrier of the reaction is a few electronvolts. As was mentioned before, the excited silver atoms represent 6% of the total neutral flux [47].

This fraction is more than one order of magnitude larger than the silver ion flux. Therefore, from a purely statistical viewpoint, associative ionization induced by excited silver atoms should be favored with respect to silver ion–molecule association.

Although detailed calculations have not been performed for all the metals considered in Section 3.1 of this article, it is possible to make some predictions concerning other systems on the grounds of their electronic properties. According to our findings, the efficiency of cationization in vacuo should depend on the number of excited sputtered metal atoms. This number is determined by both the probability of excitation during sputtering and the probability for an excited atom to survive while leaving the surface.

First, according to Craig et al. [49] and Wucher and coworkers [47,50], only metastable atoms with a hole in the d-shell have a good chance to keep the excitation due to screening of d-electrons by outer s/p electrons. From this viewpoint, all the metals used in the experimental study are good candidates, except Al. For comparison, Si, like Al, does not have d-electrons, and we showed that cationization is not observed with silicon substrates either [16]. The fact that Si and Al substrates do not induce cationization is consistent with our associative ionization model. With respect to the screening requirement, though, Pd also constitutes a limit case. Indeed, it does not have s-electrons in the ground state at all. A possible excited configuration is $4d^9 5s^1$, which means that the screening is done by only one s-electron.

Second, the process resulting in d-hole formation is the electron promotion via hard projectile–target atom and/or target atom-target atom collisions in the subsurface region of the substrate. The possibility of promotion and the probability of excitation depend on details of the electronic structure of a given pair. In particular, it is clear that the probability of excitation must depend on the binding energy of d-electrons. The greater the binding energy, the smaller impact parameters are needed for the promotion to occur and the lower the probability of a d-hole formation. As shown in Table 4 (first line), d-electrons of In and Pb have much greater binding energies than those of Cu, Ag, Au, and Pd. This second argument qualitatively explains why the yield of cationized molecules is comparatively lower for In and Pb substrates in the framework of our model. We believe that the dication distributions observed for Cu, Ag and Au (and to a lesser extent Pd) is a probability effect, because these metals also exhibit the highest cationized molecule yields. Detailed electronic structure calculations should be performed in each case to obtain the complete physical description needed to determine ion yields.

3.2.2.3. Associative ionization near the surface. In the above treatment, the process of benzene-excited metal atom association is assumed to occur in vacuum, out of the surface influence. The question of such an influence (electron exchange) on the yield of cationized organic molecules is still open, and requires additional data. The critical parameter defining a number of ions formed in electron exchange is the difference Δ between the ionization potential (IP) of the emitted particle and the work function of the substrate Φ, $\Delta = \mathrm{IP} - \Phi$ [51]. When $\Delta > 0$, which is the case for atomic sputtering of pure metals, the ion fraction in the total sputtering flux is low ($<10^{-3}$). On the other hand, when $\Delta < 0$, e.g., for alkali metal sputtering, the ion fraction approaches unit value. Typical ionization potentials for hydrocarbons are around 9 eV. Although for organometallics, IP is less than that of the constituents atoms, it is, as a rule, greater than the work functions of clean metals [52].

Table 4
Metal d-electron binding energy and strength of the organometallic bond of the $(C_6H_6 + Me)^+$ complexes (in eV)

	Al	Cr	Cu	Pd	Ag	In	Au	Pb
d-electron binding energy	–	8.3 [53]	10.6 [53]	8.5 [53]	10.4 [53]	20.4 [53]	11.7 [53]	20.9 [53]
Bond strength of C_6H_6–Me^+	1.5 [54]	1.8 [55]	2.2 [55]	?	1.7 [56]	1.0–1.3 [57]	3.0 [58]	1.4 [59]

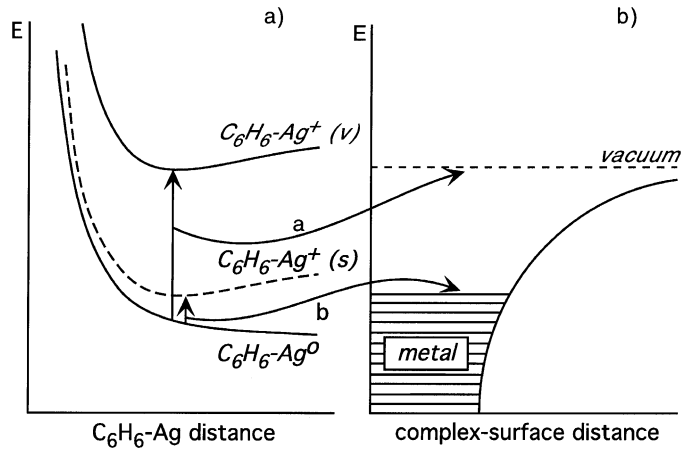

Fig. 9. Scheme representing the ionization of a C_6H_6–Ag complex in the vicinity of the surface. (a) Potential energy curves as a function of the silver atom-benzene molecule distance; (b) Energy barrier as a function of the complex-surface distance (see text for details).

It means that electron exchange should supress the yield of cationized molecules, provided that they form near the surface. However, this argument only concerns molecules being in the "zero" vibrational state. It is not the case of molecules emitted under fast ion bombardment, which have a large amount of internal energy, as shown in Section 3.2.2.4. Assuming that electronic transitions occur much faster than nuclear motions (the Frank–Condon principle), the ionization potential varies as a function of the internuclear coordinates.

An example of ionization near the surface, involving the transfer of an electron from the C_6H_6–Ag complex to the silver surface empty states, is shown in the scheme of Fig. 9. The first frame of Fig. 9 shows the potential energy of the complex as a function of the distance between its constituents, where only one degree of freedom for vibrations, along the C_6 axis, is taken into account. The second frame shows the situation of the complex with respect to the surface. In vacuum, the only possible transition leading to cationization from the ground state of the complex is transition *a*, a transition for which the energy barrier is high, as shown in Fig. 8. When the complex experiences the influence of the surface, however, the possibility for a d-electron of the silver atom to be transferred to the surface might be significant (transition *b*). The modification of the final state energy with decreasing complex-surface distance is qualitatively expressed by the translation of the C_6H_6–Ag^+ potential energy from the 'v' curve to the 's' curve in Fig. 9a. The 'v' curve represents the limiting behavior for a complex completely isolated from the metal surface and the 's' curve is related to the case where the complex lies in the vicinity of the surface. All the intermediate curves are allowed. In these conditions, ionization of the complex becomes realistic even with a ground state Ag atom because the proximity of the surface biases the energy barrier. Ionization will also be favored if the organic molecule is vibrationally excited.

In summary, the schematic view depicted in Fig. 9 qualitatively suggests that, close to the metal surface, the transition energy required for ionization of the silver atoms is not well defined. Vibrationally excited molecules might favor an electron transition from the complex to the surface, i.e., to induce cationization.

3.2.2.4. Kinetic and internal energy distributions of sputtered molecules. MD simulations indicate that metal atoms and organic molecules recombine in the course of the emission process, following the development of large-scale collective motions in the sample surface. In these concerted emission events, the organic molecule and the metal atom often have

very similar center of mass velocities. However, we showed above that they have to overcome a potential barrier of a few electronvolts to recombine. Therefore, they must have a certain amount of relative kinetic energy available for the reaction to occur. In this subsection, we propose that the energy stored in the rotational and vibrational modes of the organic molecule might be sufficient to overcome the reaction barrier.

Previous theoretical studies have shown that KED shapes are well predicted by the MD model [14,40]. In Fig. 10a, we plot the calculated KEDs of styrene tetramers sputtered from a molecular overlayer deposited on silver for two different bombardment energies, 1.5 and 5 keV. The two curves match almost perfectly and reproduce the experimental distributions measured under 12 keV Ga^+ bombardment [16]. In other words, in this projectile energy range, the KEDs are almost independent of the bombardment conditions. For this reason, we are convinced that the KEDs of Fig. 10a reasonably model our present experiments with silver substrates.

The internal energy distributions, calculated as the sum of the potential and kinetic energies of the molecule constituents in the center of mass system, are plotted in Fig. 10b for styrene tetramers. As was the case for the KEDs, the internal energy distributions are not significantly dependent on the projectile energy. They peak around 10 eV and extend beyond 25 eV. In addition, the comparison with benzene [40], biphenyl [41] and dibenzanthracene [42] molecules indicates that the average internal energy increases with the molecular weight. Hence, broader internal energy distributions are to be expected for larger styrene oligomers.

Regarding the interaction of metal atoms and organic molecules, such internal energy values should be sufficient to overcome the potential barrier for association. Because of the rotational and vibrational excitation of the sputtered molecules, a metal atom travelling along with, or within, an organic molecule, as observed in the molecular dynamics, should be able to approach the molecule enough to reach the crossing point at which the system becomes autoionizing.

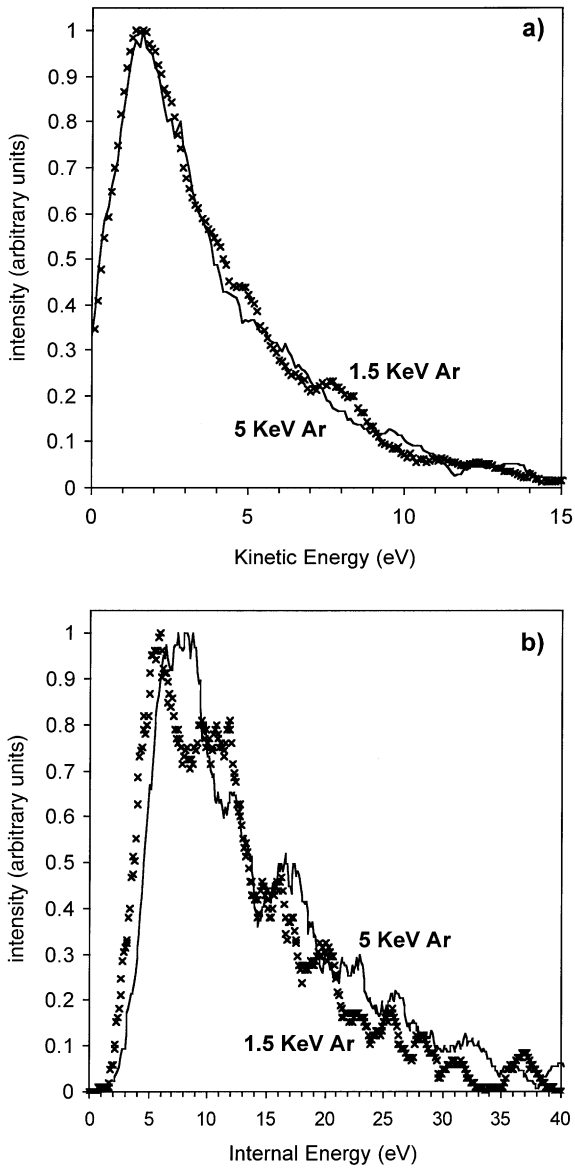

Fig. 10. Calculated energy distributions of styrene tetramers desorbed from silver substrates under 5 keV Ar bombardment. (a) Kinetic energy; (b) Internal energy.

3.2.2.5. Stability of the complex. The association process described above constitutes a low-energy cost alternative with respect to intrinsic ionization. Nonetheless, this decrease of the ionization energy should occur at the expense of the molecular species

stability. Because the association process adds a weaker bond to the molecule, the lowest energy barrier for unimolecular dissociation should be similarly reduced. In this context, the value of the binding energy between the metal and the molecule, i.e., the depth of the potential well in Fig. 8, should also be a relevant parameter to interpret ion yields. For comparison with the silver case, the binding energy of the other metal atoms in the $(C_6H_6 + Me)^+$ complexes, collected mostly from the literature, are listed in Table 4 (second line). No accurate value could be found for $(C_6H_6 + Pd)^+$ complexes. Nevertheless, the binding energy of Pd to benzene should be greater than those observed for other transition metal compounds, because Pd does not have outer s-electrons. Indeed, the interaction of a metal atom s-electron with benzene valence electrons is repulsive (Pauli repulsion) and, therefore, adding electrons to the s-outer orbital weakens the bond. Table 4 shows that copper, silver and gold have larger binding energies than indium and lead. Hence, the stability of indium and lead complex cations and dications should be lower, which is consistent with the lower cluster yields measured in the experiment (Fig. 5a). The case of chromium, however, cannot be explained by this simple argument.

In summary, the complete prediction of ion yields would require to combine the relevant parameters through a detailed treatment involving electronic structure calculation (formation probability) and internal energy dependent fragmentation (survival probability) for all the considered systems. Even though such a comprehensive study is outside the scope of this article, it has been shown that the observed experimental yields are consistent with our associative ionization model.

4. Conclusion

Metal-cationization of organic molecules occurs with different metal substrates including Cr, Cu, Pd, Ag, In, Au and Pb. The cationization efficiency varies as a function of the chosen substrate–analyte pairs. In the considered sample set, the yield of metal ions is several orders of magnitude lower than that of atoms and it is not correlated with the yield of cationized molecules.

For polymers based on the styrene structural unit, double cationization by two metal particles is also observed with several substrates, e.g., copper, silver, gold, and to a lesser extent, palladium. These substrates are those for which single cationization is also the most efficient. Therefore, the formation of dications from such surfaces can be seen as a probability effect rather than the consequence of a specific mechanism.

These results support an ionization scheme in which neutral molecules and metal atoms ionize via association above the surface. In this scenario, ionization and formation of the complex coincide, provided that the constituents approach closely enough to cross the critical distance at which the ionic state of the metal particle becomes thermodynamically favored. The metal atom in an auto-ionizing state will decay by electron emission, thereby releasing the reaction energy and locking the complex in the ionic state.

Acknowledgements

The authors thank Karsten Reihs (Bayer Ag, Leverkusen, Germany) who kindly provided the deuterated PS sample. AD and XG acknowledge the Belgian Fonds National pour la Recherche Scientifique for financial support. IW acknowledges the SSTC (Belgium) for financial support. The financial support of the National Science Foundation through the Chemistry Division, the CRIF program and the MRI program are gratefully acknowledged by AD and BJG. This work was partly supported by the Action de Recherche Concertée (01/06-269) of the Communauté Française de Belgique. The ToF-SIMS equipment was acquired with the support of the Région Wallonne and FRFC-Loterie Nationale of Belgium. Electronic structure computations were performed using facilities provided by the FRFC project no. 2.4556.99. In Penn State, additional computational resources were provided in part by the IBM

Selected University Resource Program and the Center for Academic Computing of Penn State University.

References

[1] A. Benninghoven, P. Bertrand, H.-N. Migeon, H.W. Werner (Eds.), SIMS XII Proceedings, Wiley, New York, 2000.
[2] B. Hagenhoff, The Static SIMS Library, in: J.C. Vickerman, D. Briggs, A. Henderson (Eds.), Surface Spectra, Manchester, 1997, p. 39.
[3] A.I. Gusev, B.K. Choy, D.M. Hercules, J. Mass Spectrom. 33 (1998) 480.
[4] R.W. Linton, M.P. Mawn, A.M. Belu, J.M. DeSimone, M.O. Hunt Jr., Y.Z. Menceloglu, H.G. Cramer, Surf. Interface Anal. 20 (1993) 991.
[5] K.J. Wu, R.W. Odom, Anal. Chem. 68 (1996) 873.
[6] H. Grade, N. Winograd, R.G. Cooks, J. Am. Chem. Soc. 99 (1977) 7725.
[7] H. Grade, R.G. Cooks, J. Am. Chem. Soc. 100 (1978) 5615.
[8] I.V. Bletsos, D.M. Hercules, D. van Leyen, A. Benninghoven, Macromolecules 20 (1987) 407.
[9] P.A. Zimmerman, D.M. Hercules, Appl. Spectrosc. 47 (1993) 1545.
[10] A. Benninghoven, B. Hagenhoff, E. Niehuis, Anal. Chem. 65 (1993) 630A.
[11] K. Xu, A. Proctor, D.M. Hercules, Mikrochim. Acta 122 (1996) 1.
[12] A.J. Nicola, D.C. Muddiman, D.M. Hercules, J. Am. Soc. Mass Spectrom. 7 (1996) 467.
[13] D. Pleul, F. Simon, H.-J. Jacobasch, J. Fresenius, Anal. Chem. 357 (1997) 684.
[14] A. Delcorte, X. Vanden Eynde, P. Bertrand, J.C. Vickerman, B.J. Garrison, J. Phys. Chem. B104 (2000) 2673.
[15] A. Delcorte, B.J. Garrison, J. Phys. Chem. B104 (2000) 6785.
[16] A. Delcorte, P. Bertrand, Surf. Sci. 412/413 (1998) 97.
[17] W. Husinsky, G. Betz, Thin Solid Films 272 (1996) 289.
[18] G. Betz, C. Dandachi, W. Husinsky, Izvestia Akademii Nauk: Seria Fizicheskaja 62 (1998) 690.
[19] G. Betz, W. Husinsky, in: A. Benninghoven, P. Bertrand, H.-N. Migeon, H.W. Werner (Eds.), SIMS XII Proceedings, Wiley, New York, 2000, p. 13.
[20] B.J. Garrison, A. Delcorte, K.D. Krantzman, Acc. Chem. Res. 33 (2000) 69.
[21] B.W. Schueler, Microsc. Microanal. Microstruct. 3 (1992) 119.
[22] A. Delcorte, X. Vanden Eynde, P. Bertrand, D.F. Reich, Int. J. Mass Spectrom. 189 (1999) 133.
[23] J.P. Biersack, in: P. Mazzoldi, G.W. Arnold (Eds.), Ion Beam Modification of Insulators, Elsevier, Amsterdam, 1987, p. 26.
[24] http://www.research.ibm.com/ionbeams/SRIM/.
[25] D.R. Lide (Ed.), Handbook of Chemistry and Physics, CRC Press, New York, 1995.
[26] D.W. Brenner, Phys. Rev. B42 (1990) 9458.
[27] D.W. Brenner, J.A. Harrison, C.T. White, R.J. Colton, Thin Solid Films 206 (1991) 220.
[28] I. Wojciechowski, A. Delcorte, X. Gonze, P. Bertrand, Chem. Phys. Lett. 346 (2001) 1.
[29] S. Goedecker, SIAM J. Sci. Comput. 1 (1997) 1605.
[30] M.C. Payne, M.P. Teter, D.C. Allan, T.A. Arias, J.D. Joannopoulos, Rev. Mod. Phys. 64 (1992) 1045.
[31] X. Gonze, Phys. Rev. B54 (1996) 4383.
[32] M. Fuchs, M. Scheffler, Comput. Phys. Commun. 119 (1999) 67.
[33] O. Gunnarson, B.I. Lundqvist, Phys. Rev. B43 (1991) 1993.
[34] http://www.webelements.com.
[35] S. Baier, M. Martins, B.R. Müller, M. Schulze, P. Zimmerman, J. Phys. B23 (1990) 3095.
[36] A. Wucher, W. Berthold, H. Oechsner, K. Franzreb, Phys. Rev. A49 (1994) 2188.
[37] W.H. Press, B.P. Flannery, S.A. Teukolsky, W.T. Vetterling, Numerical Recipes (FORTRAN Version), Cambridge University Press, Cambridge, 1989.
[38] Y.-P. Ho, Y.-C. Yang, S.J. Klippenstein, R.C. Dunbar, J. Phys. Chem. A101 (1997) 3338.
[39] A. Delcorte, P. Bertrand, B.J. Garrison, J. Phys. Chem. B105 (2001) 9474.
[40] R. Chatterjee, Z. Postawa, N. Winograd, B.J. Garrison, J. Phys. Chem. B103 (1999) 151.
[41] J.A. Townes, A.K. White, E.N. Wiggins, K.D. Krantzman, B.J. Garrison, N. Winograd, J. Phys. Chem. B103 (1999) 4587.
[42] A. Delcorte, P. Bertrand, J.C. Vickerman, B.J. Garrison, in: A. Benninghoven, P. Bertrand, H.-N. Migeon, H.W. Werner (Eds.), SIMS XII Proceedings, Elsevier, Amsterdam, 2000, p. 27.
[43] D.M. Hercules, J. Mol. Struct. 292 (1993) 49.
[44] K.S.S. Liu, C.W. Yong, B.J. Garrison, J.C. Vickerman, J. Phys. Chem. B103 (1999) 3195.
[45] I.A. Hornbeck, J.P. Molnar, Phys. Rev. 84 (1951) 621.
[46] H.H. Andersen, H.L. Bay, in: R. Behrisch (Ed.), Sputtering by Particle Bombardment I, Springer, Berlin, 1981, p. 145.
[47] W. Berthold, A. Wucher, Phys. Rev. Lett. 76 (1996) 2181.
[48] V. Philipsen, private communication.
[49] B.I. Craig, J.P. Baxter, J. Singh, G.A. Schick, P.H. Kobrin, B.J. Garrison, N. Winograd, Phys. Rev. Lett. 57 (1986) 1351.
[50] A. Wucher, Z. Sroubek, Phys. Rev. B55 (1997) 780.
[51] M. L. Yu, in: R. Behrish, K. Wittmaack (Eds.), Sputtering by Particle Bombardment III, Springer, Berlin, 1991, p. 412.
[52] R. Pandey, B.K. Rao, P. Jena, M.A. Blanco, J. Am. Chem. Soc. (2001).
[53] www.chembio.uoguelph.ca/educmat/atomdata/bindener/elec-bind.html.
[54] R.C. Dunbar, S.J. Klippenstein, J. Hrusak, D. Stockigt, H. Schwarz, J. Am. Chem. Soc. 118 (1996) 5277.
[55] S.J. Klippenstein, C.-N. Yang, Int. J. Mass. Spectrom. 201 (2000) 253.
[56] Y.-P. Ho, Y.-C. Yang, S.J. Klippenstein, R.C. Dunbar, J. Phys. Chem. A101 (1997) 3388.
[57] S. Arulmozhiraja, T. Fujii, H. Tokiwa, Chem. Phys. 250 (1999) 237.
[58] D. Schröder, H. Schwarz, J. Hrusak, P. Pyykkö, Inorg. Chem. 37 (1998) 624.
[59] I. Wojciechowski, private communication.